DOI: 10.1002/cphc.2006

Oriented Growth of Single Crystalline Bi_2S_3 Nanowire Arrays

Ju Xu[a], Nikolay Petkov[a], Xueyan Wu[a], Daniela Iacopino[b], Aidan J. Quinn[b], Gareth Redmond[b], Thomas Bein[c], Michael A. Morris[a] and Justin D. Holmes* [a]

Various approaches, including electrochemical and electroless deposition, sol-gel, paired-cell, chemical vapour deposition, and supercritical fluid deposition, have been utilised to produce a range of inorganic nanowires, including metals, metal oxides and semiconductors within the channels of anodic alumina membranes (AAMs). [1-4] However, these methods typically produce amorphous or polycrystalline nanowires with poorly defined structures.[5] Post-treatment of these nanowires, e.g. by annealing at elevated temperatures, is often required to achieve the desired crystallinity and mechanical integrity necessary for many applications.[6, 7] Electrodeposition techniques have been used to obtain ordered single crystal arrays of metal and II-VI nanowires within AAMs.[8-16] However, a significant limitation of this synthetic approach is that it requires the deposited material to be both easily reduced and conductive.[17] Also, the optimal deposition conditions depend on the metal or compound to be deposited, which may restrict the compositional variety of the single crystal nanowires that can be formed. Several compounds such as CdS, TiO_2, $YBa_2Cu_3O_{7-\delta}$, with a single crystal structure, have also been obtained as nanowire arrays in AAMs using direct sol-gel or electric field assisted sol-gel methods.[5, 18, 19] But, the low filling efficiency is still the main problem because nanomaterials usually experienced a serious shrinkage and cracking due to the low concentration of the sol. Besides, the rough surfaces and many domain boundaries of the TEM images were quite normally found on the obtained single crystal nanowires using both electrodeposition and sol-gel approaches, and PXRD results also showed a nonconsistent growth direction. [5, 8-16, 18-20] A pressure injection process for single crystal nanowire arrays has also been reported by Zhang et al.[21] for the synthesis of low melting point metal nanowires, e.g. Bi, Sn, In, Al,[21, 22] but this method only limited to some low melting point metals e.g. Bi, Sn, In, Al[21, 22]due to the deformation of the template at high temperature.[21] Thus, it is still a big challenge to fabricate arrays of oriented single crystal nanowires, with high aspect ratios, within the AAM templates. [5, 14, 16, 18, 23]

Bi_2S_3, an ionic n-type semiconductor with a direct band gap of 1.3 eV, has numerous potential applications as a material for photovoltaic[24, 25] and thermoelectric[26] devices. Several techniques have previously been reported for synthesizing randomly oriented Bi_2S_3 nanowires including solvothermal and hydrothermal decomposition,[27-29] microwave irradiation,[30] crystallization of amorphous colloids,[31] chemical vapor deposition,[32] sonochemical,[33] solventless,[34]and ionic liquid-assisted methods.[35] Polycrystalline Bi_2S_3 nanowires embedded inside the channels of AAMs have also been reported by electrochemical deposition[20] and photochemical synthesis.[36] To date, there have been no reports in the literature of the templated growth of arrays of single crystal B_2S_3 nanowires.

In this communication we demonstrate a new and simple template-based solventless approach, without the use of a catalyst or complexing agent, to synthesize single crystal Bi_2S_3 nanowires inside the channels of AAMs by the thermolysis of a single source precursor. A high yield of pore filling, more than 80 %, of Bi_2S_3 nanowires inside the channels of the template can be achieved by injection of the melted precursor liquid into the channels followed by thermolysis. X-ray diffraction (XRD) and high resolution transmission electron microscopy (HRTEM) studies suggest that

[a] Ju Xu, Dr. Nikolay Petkov, Dr. Xueyang Wu, Prof. Michael A. Morris, Dr. Justin D. Holmes
Department of Chemistry,
Materials Section and Supercritical Fluid Centre,
University College Cork, Cork, Ireland.
Tel: +353 (0)21 4903608; Fax: + 353 (0)21 4274097;
E-mail: j.holmes@ucc.ie

[b] Dr. Daniela Iacopino, Dr. Aidan J. Quinn, Dr. Gareth Redmond
Nanotechnology Group,
Tyndall National Institute,
Lee Maltings, Cork, Ireland.

[c] Prof. Thomas Bein
Department of Chemistry and Biochemistry ,
University of Munich,Butenandtstr.5-13 (E),
81377 Munich, Germany

Supporting information for this article is available on the WWW under http://www.chemphyschem.org or from the author

highly oriented growth of the Bi_2S_3 nanowires, with respect to the channel direction of the AAM, can be achieved. Additionally, the mean diameter of the nanowires can readily be controlled by using AAMs with different pore diameters. The absorption profile (band-gap) of these nanowires was found to be blue-shifted to higher energies as the mean diameter of the nanowires decreased.

Bismuth bis(diethyldithiocarbamate) $[Bi(S_2CNEt_2)_3]$ complex, a organometallic molecular which was normally used in preparation thin film by a MOCVD method[37] was chosen as a single source precursor to make the nanowire arrays within the AAM templates. The precursor has a mild melting point temperature, about 200°C, and decomposition temperature around 300 °C, which make it an ideal liquid precursor after melting to be injected within the pores of the AAM template.

AAMs with mean pore diameters of approximately 80 and 20 nm were used as hard templates for the synthesis of arrays of Bi_2S_3 nanowires. An XRD pattern of the as-decomposed material on the membrane surface shows a number of reflections that can be indexed to the orthorhombic bismuthinite structure (reference pattern, JCPDS No. 170320) (Figure 1a). The XRD patterns from the polished membranes, i.e the surface material has been removed leaving the material decomposed within the pores only, show one very high intensity reflection emanating from the (002) set of planes, at 48.2 2θ degrees, indicating that the Bi_2S_3 nanowires have a highly preferential orientation along the [002] direction (Figure 1b and c). This remarkable difference in the XRD characteristics of the Bi_2S_3 crystals on the surface *vs* the polished samples can be explained by the fact that in the reflection XRD experiment (θ - 2θ) only the crystallographic planes parallel to the sample surface can be detected. Thus randomly oriented Bi_2S_3 crystals on the membrane surface give rise to powder-like patterns whereas the preferentially oriented nanowires inside the channels of the AAMs results in a reduced number of reflections, corresponding to planes parallel to the membrane surface, i.e the (200) reflection.

Side-view scanning electron microscopy (SEM) images of the samples subjected to thermolysis at 300°C reveal that continuous Bi_2S_3 nanowires protrude out of the channels of the AAMs upon breakage of the membranes (Figure 2a and b). The nanowires are embedded and restricted by the dimensions of the membrane channels, and at the same time isolated from each other inside the porous alumina matrix. The TEM images of the liberated nanowires show lengths of up to tens of micrometers and mean diameters of approximately 80 nm and 20 nm, depending on the AAM used as the template (Figure 3a and b). X-ray energy dispersion analysis (EDAX) shown in support information reveals that the nanowires are composed of Bi and S, no Al were detected suggesting the template were completely dissolved, quantitative analysis result indicates that the atomic composition is close to 3:2 stoichiometry. The nanowires show very smooth surface and very few defects unlike nanowires obtained from electrodeposition or sol-gel methods in most publications. [5, 8-16, 18-20, 38, 39] Small gaps between the nanowires and the walls of columnar channels of the AAMs were observed in the plane-view TEM images (Figure 4 a and b). Nanowire growth inside the channels of the AAMs probably occurs through an anisotropic growth due to the highly anisotropic crystalline structure of Bi_2S_3. The role of the porous template is to separate and isolate the nanowires in an ordered array. The reduced dimensions of the nanowires in diameter compared to the dimensions of the pores, can be explained by volume contraction during the crystallization process as well as by non-uniform filling of the pores with the melted precursor. Thus the nanowires show a little broader distribution of diameters than the channel size distribution of the templating membranes, such as 10-80 nm for the 80 nm membranes and 8-20 nm for the 20 nm membranes, respectively (the pore size and nanowire diameter distributions were calculated from at least 5 different plane-view TEM images). The total pore filling ratio calculated by the plane view TEM images is about 80 %, densities of 1.5×10^9 and 8.0×10^9 nanowires per cm^2, for the 80 and 20 nm membranes respectively, can be obtained.

The crystal structure of the Bi_2S_3 nanowires was examined by selected area electron diffraction (SAED) and HRTEM combined with fast fourier transforms (FFTs). To help interpret the SAED and FFTs patterns, electron diffraction patterns were simulated with a crystal studio software package using appropriate orthorhombic unit cell dimensions with a P*bmn* space group. Figure 5 shows TEM images of 60 and 15 nm Bi_2S_3 nanowires, isolated from both types of membranes

under study, respectively. The corresponding SAED patterns verify their single crystalline nature indicated by the sharp diffraction dots. The SAED patterns were taken with the electron beam along the [010] direction and confirmed that the nanowires were grown along the [002] direction (in line with XRD data). The HRTEM images shown in Figure 5(b) and 5(d) also provide evidence of the single crystalline nature of the nanowires with clearly visible lattice fringes. For example in Figure 5(b), lattice fringes with a d-spacing of about 5.6 Å, attributed to the (200) lattice planes, are observed parallel to the growth direction of the nanowires. The FFTs of the HRTEM shown in Figure 5(b) and 5(d) further validate the [002] growth direction of the nanowires. All of the nanowires (about 10-15 nanowires) that we studied by SAED and FFTs of the HRTEM images, islolated from both types of membranes, showed growth directions along the [002] zone axis. These data are in good agreement with the XRD results reported in the literature for single crystalline Bi_2S_3 nanowires and nanorods grown by various methods.[29, 34, 40]

To further confirm the orientation of the nanowires inside the anodic alumina channels, Bi_2S_3 nanowires were imaged inside the AAMs (Figure 6) with the electron beam along the direction of the channels (parallel to the growth direction). The results show that both the FFTs of the HRTEM images and the SAED patterns can be indexed assuming the beam is incident along the [002] direction (several tens of SAED and FFTs were recorded and compared to simulated patterns). This result is in consistent with XRD, SAED and HRTEM analysis presented above and further confirms the alignment of the single crystalline Bi_2S_3 nanowires with a [002] growth direction parallel to the long axis of the channels of the AAMs.

Figure 7a shows the optical properties of Bi_2S_3 powder, formed by the decomposition of the precursor in the absence of a template, Bi_2S_3 nanowires within the channels of an AAM template and an empty membrane. No significant absorption arises from the unfilled AAM templates. There is an obvious blue shift of the absorption edge for the Bi_2S_3 nanowires within the 20 nm AAMs compared with the Bi_2S_3 powders and the Bi_2S_3 nanowires within the 80 nm AAMs. For a direct band gap semiconductor such as Bi_2S_3, the band gap energy is usually defined by the x-axis intercept of $(\alpha h\nu)^2$ versus $h\nu$, where α is the absorption coefficient.[41, 42] Applied to the near-edge absorption for Bi_2S_3 nanowires, Figure 7(b) shows the $(\alpha h\nu)^2$ versus $h\nu$ plot obtained from curves 1 to 3 in Figure 7(a). Extrapolation of the plot to the energy axis gives a value of approximately 1.35 eV for the band gap of the Bi_2S_3 powder. The band-gap energy of the Bi_2S_3 nanowires within the pores of the 80 and 20 nm AAMs was 1.36 and 1.51 eV respectively. The band-gap energies reported here lie between the energy range of 1.25-2.0 eV, which is similar to the energies previously reported for Bi_2S_3 thin film and nanowires.[20, 43-45] The bigger optical band gap (E_g) for the Bi_2S_3 nanowires within the 20 nm AAMs is uneasy to explain, but it may relative with quantum confinement effects of the small diameters of the nanowires since little defects were found for these nanowires according to the above results.

In summary, a solventless, template-based approach has been developed for growing high density arrays of single crystal Bi_2S_3 nanowires. The role of the porous structure is to separate, isolate these nanowires and guide their growth in an ordered array. A high loading of the melted precursor can be obtained in the channels of the AAMs, which can be subsequently crystallized to form continuous single crystal nanowires. XRD, SAED and HRTEM imaging provided evidence that the nanowires produced are preferentially oriented inside the channels of the AAMs along the [200] growth direction. By varying the pore size of the templates, the mean diameter of the nanowires can also be controlled. The absorption band gap energies of the synthesised nanowires were found to increase as the mean diameter of the nanowires decreased. By choosing suitable precursors, single crystal nanowire arrays of other materials can also be prepared using this approach. Compare with other methods, our solventless approach offers the advantages of simple experimental set-up and operation procedure, the highly preferential growth orientation with respect to the template channel direction[46] and especially for the synthesis of complex compound nanowire arrays, which is a big challenge using the normal electrodeposition approach due to its difficulty to control the reaction conditions.

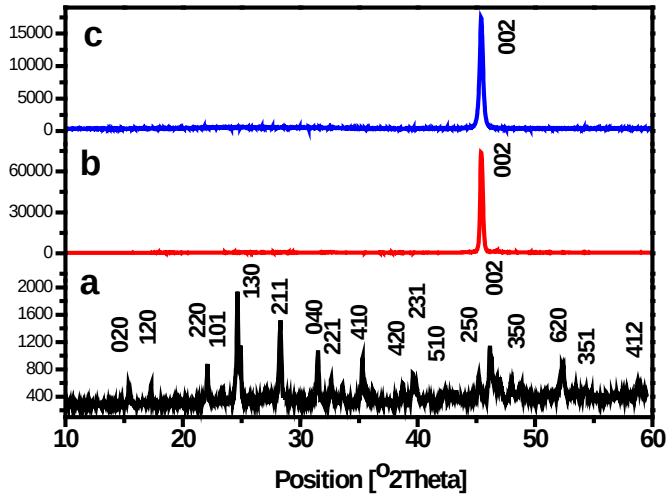

Figure 1. XRD patterns of (a) Bi_2S_3 crystals formed outside the AAM template and Bi_2S_3 nanowire arrays formed within AAMs with mean diameters of (b) 80 nm and (c) 20 nm. All samples exhibit an orthorhombic Bi_2S_3 crystal structure (bismuthinite, JCPDS file 17-0320) and the Bi_2S_3 nanowires within template have a preferred orientation along the [002] direction.

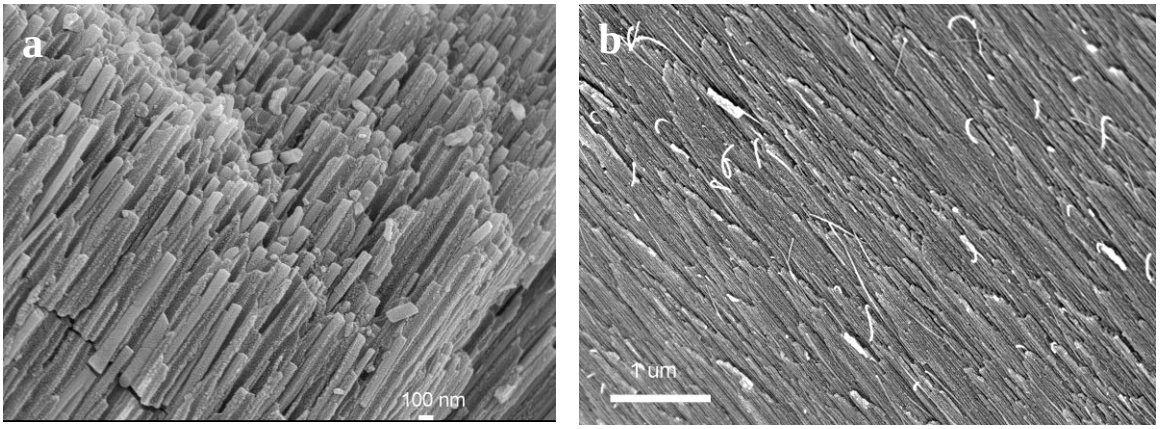

Figure 2 Side-view SEM images of the Bi_2S_3 nanowire arrays within AAMs with mean pore diameters of a) 80 nm and b) 20 nm.

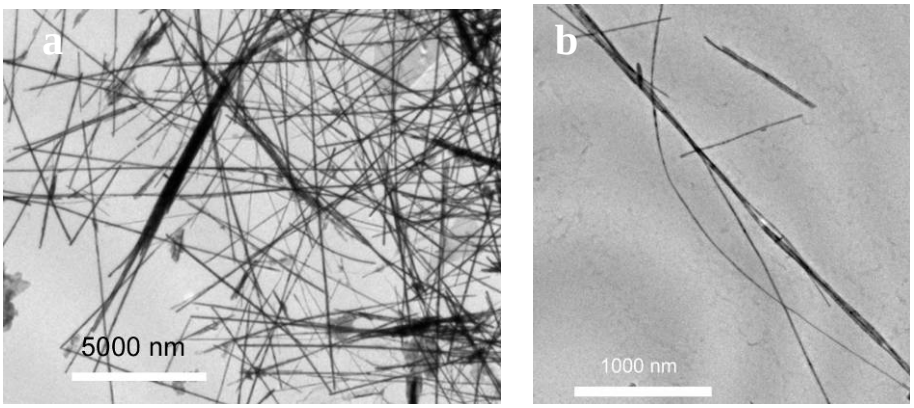

Figure 3 TEM images of Bi_2S_3 nanowires liberated from AAMs with mean pore diameters of a) 80 nm and b) 20 nm.

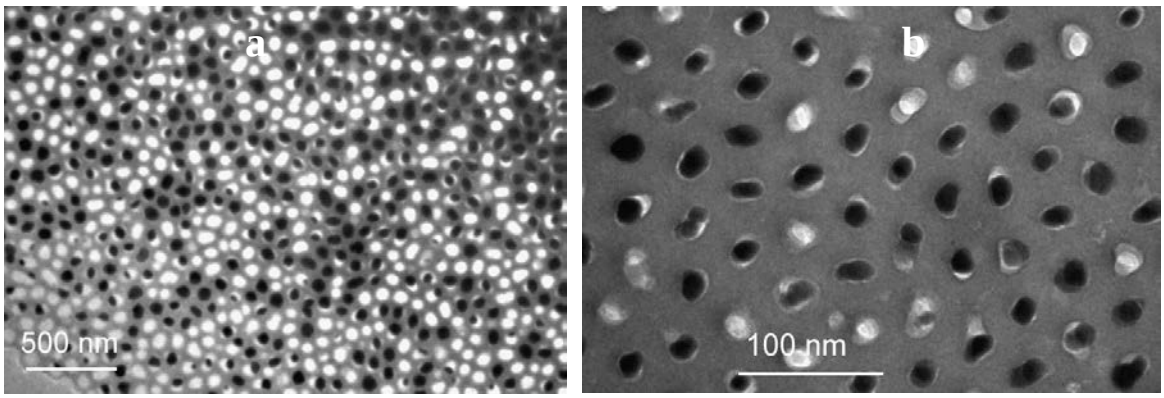

Figure 4 Plane-view TEM images of the Bi_2S_3 nanowire arrays within the pores of a) 80 nm and b) 20 nm AAMs.

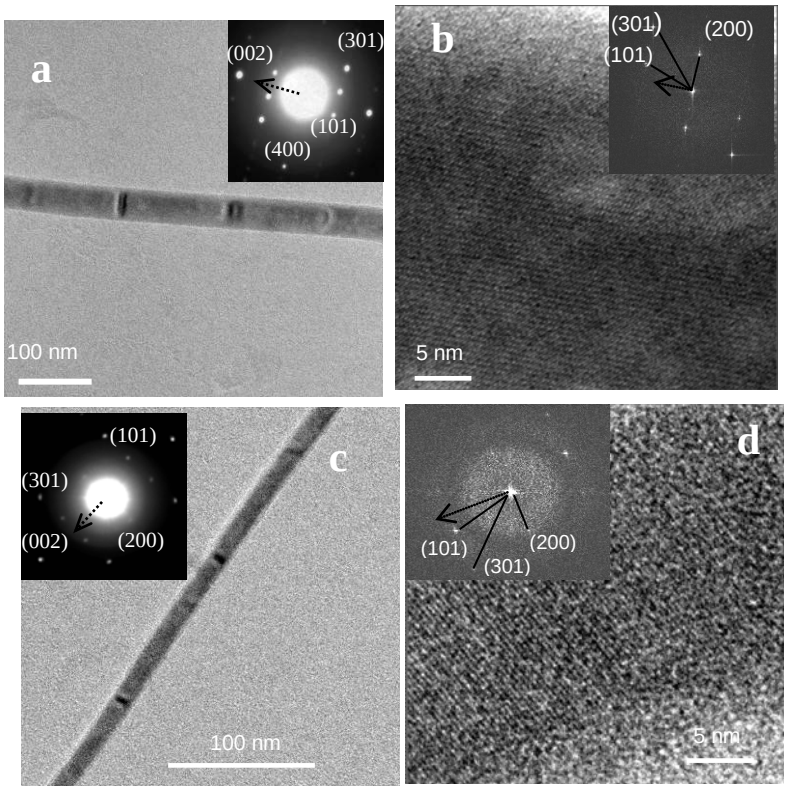

Figure 5 HRTEM images with the corresponding SAED and FFTs for isolated Bi_2S_3 nanowires with diameters of about 60 nm and 15 nm (insets: SAED and FFTs are indexed in the the P*bmn* space group with the electron beam along the [010] direction, the arrows show the growth direction of the nanowires that is along the [002] zone axis).

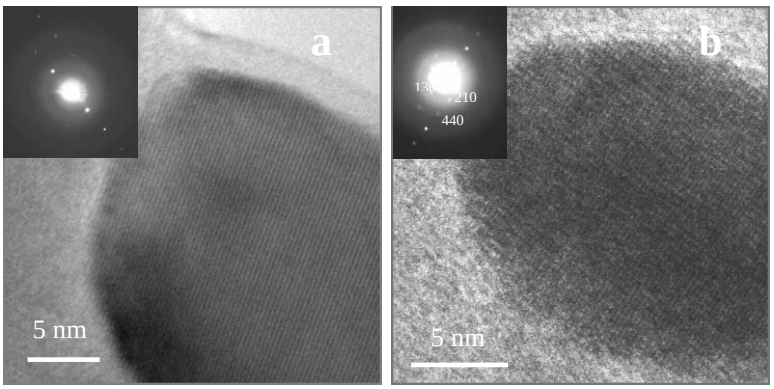

Figure 6 Plan-view HRTEM images of Bi_2S_3 nanowires inside the channels of the AAMs with mean pore diameters of a) 80 nm and b) 20 nm (inset is the corresponding SAED, indexed in the *Pbmn* space group with the electron beam along the [002] direction).

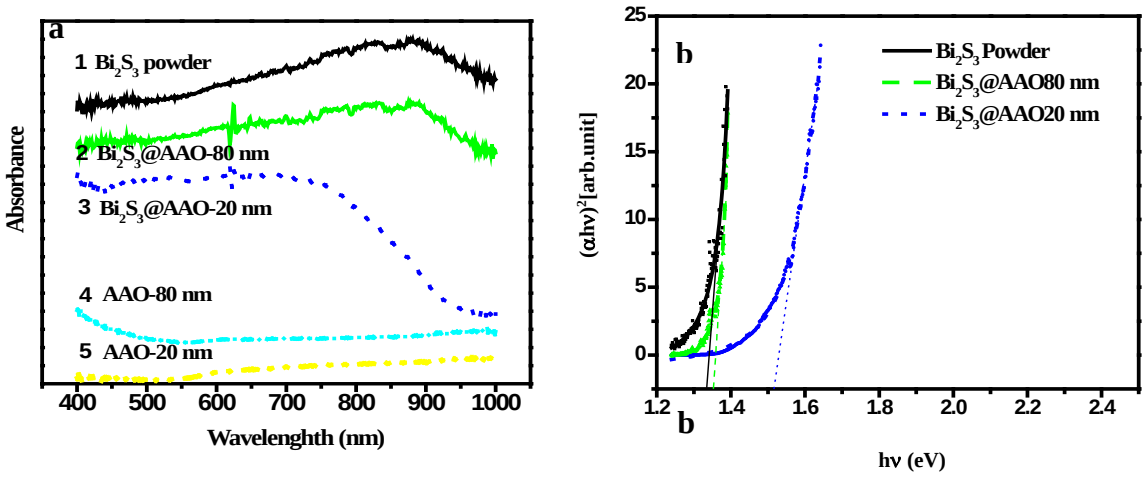

Figure 7 a) Absorption spectra of Bi_2S_3 powder, Bi_2S_3 nanowires inside AAM templates and a blank AAM membrane, (b) $(\alpha h\nu)^2$ versus $h\nu$ obtained from curves 1,2,3 shown in (a).

Experimental Section

Sample preparation: The single source precursor, bismuth bis(diethyldithiocarbamate) [$Bi(S_2CNEt_2)_3$] complex was prepared by the reaction of Bi_2O_3 with carbon disulfide and diethylamine in methanol and was thoroughly purified by repeated recrystallization as described by Monteiro *et al.* .[47] The AAMs were made in-house using a well known two-step anodization procedure described elsewhere [4, 48]. The synthesis of single crystal Bi_2S_3 nanowire arrays was carried out in a flat bottom glass tube (inner diameter 14 cm). In a typical experiment, the organometallic precursor (~300 mg) was put on the surface of the AAM in the glass tube. The tube was then heated to 200 ˚C under vacuum. After the precursor melted, the temperature was maintained for another 30 minutes. The vacuum was then disconnected and the glass tube containing the sample was placed on a hot plate at 300 ˚C for 30 minutes until the Bi_2S_3 precursor had completely decomposed. The layer of Bi_2S_3 formed on the surface of the template was removed by polishing with 5 µm diamond paste and washing with acetone whilst sonicating. The back aluminium metal of the AAM was removed using a saturated copper (II) chloride solution. The templates were dissolved completely with a 6 M aqueous solution of sodium hydroxide at 60°C. The resulting suspension was washed with deionized water several times.

X-ray diffraction measurements: XRD measurements were performed with a Philips X'Pert diffractometer using Cu $K\alpha_1$ radiation with an anode current of 35 mA and an accelerating current of 40 kV. The measurements were done in reflection ($(\theta - 2\theta)$ geometry.

Electron microscopy: SEM images of the broken Bi_2S_3 filled AAM templates, put on conductive carbon tape, were obtained using a field-emission scanning electron microscope JEOL JSM 6700F at an accelerating voltage of 5kV. The TEM and electron diffraction images were investigated in a JEOL JEM-2000FX microscope operated at 200 kV. The sample was dispersed in absolute ethanol, sonicated and dropped onto copper grids coated with a holey carbon film. The plane-view TEM samples were made after mechanical polishing both sides of the template, followed by Ar-ion milling until the sample was transparent for TEM imaging. High-resolution TEM images were recorded with a Joel JEM 2010 microscope operating at 200 kV.

Optical measurements: Absorption measurements on the samples, attached to a quartz plate with wax, were made using an Agilent 8453E UV-Visible spectrophotometer with a Labsphere RSA-HP-53 diffuse reflectance and transmittance accessory.

Acknowledgement

The authors acknowledge financial support for their work from the Higher Education Authority (HEA) in Ireland under PRTLI 3 funding and Science Foundation Ireland (Grant 03/IN3/I375). We are greatful to Joseph Tobin for some TEM analysis and Brain Daly for useful discussions.

Keywords: Nanowire arrays, Bi_2S_3, Template, Solventless, single source precursor

[1] V. SADASIVAN, C. P. RICHTER, L. MENON, P. F. WILLIAMS, *Aiche J.* **2005**, *51*, 649-655.
[2] S. SHINGUBARA, *J. Nanopart. Res.* **2003**, *5*, 17-30.
[3] Y. PIAO, H. LIM, J. Y. CHANG, W. Y. LEE, H. KIM, *Electrochim. Acta* **2005**, *50*, 2997-3013.
[4] D. ERTS, B. POLYAKOV, B. DALYT, M. A. MORRIS, S. ELLINGBOE, J. BOLAND, J. D. HOLMES, *J. Phys. Chem. B* **2006**, *110*, 820-826.
[5] H. Q. CAO, Y. XU, J. M. HONG, H. B. LIU, G. YIN, B. L. LI, C. Y. TIE, Z. XU, *Adv. Mater.* **2001**, *13*, 1393-1394.
[6] H. LI, C. L. XU, G. Y. ZHAO, H. L. LI, *J. Phys. Chem. B* **2005**, *109*, 3759-3763.
[7] G. B. JI, J. M. CAO, F. ZHANG, G. Y. XU, H. L. SU, S. L. TANG, B. X. GU, Y. W. DU, *J. Phys. Chem. B* **2005**, *109*, 17100-17106.
[8] C. JIA, W. F. LIU, C. G. JIN, B. ZHANG, L. Z. YAO, W. CAI, X. G. LI, *Chem. Lett.* **2004**, *33*, 634-635.
[9] L. LI, Y. ZHANG, G. H. LI, L. D. ZHANG, *Chem. Phys. Lett.* **2003**, *378*, 244-249.
[10] C. G. JIN, W. F. LIU, C. JIA, X. Q. XIANG, W. L. CAI, L. Z. YAO, X. G. LI, *J. Cryst. Growth* **2003**, *258*, 337-341.
[11] Y. T. PANG, G. W. MENG, L. D. ZHANG, W. J. SHAN, X. Y. GAO, A. W. ZHAO, Y. Q. MAO, *J. Phys.-Condes. Matter* **2002**, *14*, 11729-11736.
[12] J. ZHANG, L. D. ZHANG, X. F. WANG, C. H. LIANG, X. S. PENG, Y. W. WANG, *J. Chem. Phys.* **2001**, *115*, 5714-5717.
[13] D. S. XU, Y. J. XU, D. P. CHEN, G. L. GUO, L. L. GUI, Y. Q. TANG, *Chem. Phys. Lett.* **2000**, *325*, 340-344.
[14] C. JIA, B. ZHANG, W. F. LIU, C. G. JIN, L. Z. YAO, W. L. CAI, X. G. LI, *J. Cryst. Growth* **2005**, *285*, 527-533.
[15] C. G. KUO, S. C. LO, J. H. CHEN, C. C. CHIANG, C. G. CHAO, *Jpn. J. Appl. Phys. Part 1 - Regul. Pap. Brief Commun. Rev. Pap.* **2005**, *44*, 3333-3336.
[16] L. LI, Y. W. YANG, X. H. HUANG, G. H. LI, L. D. ZHANG, *J. Phys. Chem. B* **2005**, *109*, 12394-12398.
[17] E. K. P. SARAH J. HURST, LIDONG QIN, CHAD A. MIRKIN,, *Angew. Chem. Int. Ed.* **2006**, *45*, 2672.
[18] Z. MIAO, D. S. XU, J. H. OUYANG, G. L. GUO, X. S. ZHAO, Y. Q. TANG, *Nano Lett.* **2002**, *2*, 717-720.
[19] J. XU, X. H. LIU, Y. D. LI, *Mater. Chem. Phys.* **2004**, *86*, 409-413.
[20] X. S. PENG, G. W. MENG, J. ZHANG, L. X. ZHAO, X. F. WANG, Y. W. WANG, L. D. ZHANG, *J. Phys. D-Appl. Phys.* **2001**, *34*, 3224-3228.
[21] Z. ZHANG, D. GEKHTMAN, M. DRESSELHAUS, J. YING, *Chem. Mater.* **1999**, *11*, 1659-1665.
[22] C. C. CHEN, Y. BISRAT, Z. P. LU, R. E. SCHAAK, C. G. CHAO, D. C. LAGOUDAS, *Nanotechnology* **2006**, *17*, 367-374.
[23] C. G. JIN, X. Q. XIANG, C. JIA, W. F. LIU, W. L. CAI, L. Z. YAO, X. G. LI, *J. Phys. Chem. B* **2004**, *108*, 1844-1847.
[24] S. H. PAWAR, S. P. TAMHANKAR, C. D. LOKHANDE, *Mater. Chem. Phys.* **1984**, *11*, 401-412.

[25] R. S. MANE, B. R. SANKAPAL, C. D. LOKHANDE, *Mater. Chem. Phys.* **1999**, *60*, 158-162.
[26] B. X. CHEN, C. UHER, L. IORDANIDIS, M. G. KANATZIDIS, *Chem. Mat.* **1997**, *9*, 1655-1658.
[27] S. H. YU, L. SHU, J. A. YANG, Z. H. HAN, Y. T. QIAN, Y. H. ZHANG, *J. Mater. Res.* **1999**, *14*, 4157-4162.
[28] Z. P. LIU, S. PENG, Q. XIE, Z. K. HU, Y. YANG, S. Y. ZHANG, Y. T. QIAN, *Adv. Mater.* **2003**, *15*, 936-+.
[29] Y. YU, C. H. JIN, R. H. WANG, Q. CHEN, L. M. PENG, *J. Phys. Chem. B* **2005**, *109*, 18772-18776.
[30] X. H. LIAO, H. WANG, J. J. ZHU, H. Y. CHEN, *Mater. Res. Bull.* **2001**, *36*, 2339-2346.
[31] X. B. CAO, L. Y. LI, X. YI, *J. Colloid Interface Sci.* **2004**, *273*, 175-180.
[32] Y. W. KOH, C. S. LAI, A. Y. DU, E. R. T. TIEKINK, K. P. LOH, *Chem. Mat.* **2003**, *15*, 4544-4554.
[33] H. WANG, J. J. ZHU, J. M. ZHU, H. Y. CHEN, *J. Phys. Chem. B* **2002**, *106*, 3848-3854.
[34] M. B. SIGMAN, B. A. KORGEL, *Chem. Mat.* **2005**, *17*, 1655-1660.
[35] Y. JIANG, Y. J. ZHU, *J. Phys. Chem. B* **2005**, *109*, 4361-4364.
[36] W. B. ZHAO, J. H. ZHU, Y. ZHAO, H. Y. CHEN, *Mater. Sci. Eng. B-Solid State Mater. Adv. Technol.* **2004**, *110*, 307-313.
[37] O. C. MONTEIRO, T. TRINDADE, J. H. PARK, P. O'BRIEN, *Chem. Vapor Depos.* **2000**, *6*, 230-+.
[38] H. PAN, H. SUN, C. POH, Y. P. FENG, J. Y. LIN, *Nanotechnology* **2005**, *16*, 1559-1564.
[39] L. LI, Y. W. YANG, X. H. HUANG, G. H. LI, L. D. ZHANG, *Nanotechnology* **2006**, *17*, 1706-1712.
[40] Z. P. LIU, D. XU, J. B. LIANG, W. J. LIN, W. C. YU, Y. T. QIAN, *J. Solid State Chem.* **2005**, *178*, 950-955.
[41] S. A. MAHMOUD, *Physica B* **2001**, *301*, 310-317.
[42] S. S. K. KUMAR VIPIN , SHARMA T.P., SINGH V., *Opt. Mater.* **1999**, *12*, 115.
[43] M. MEDLES, N. BENRAMDANE, A. BOUZIDI, A. NAKRELA, H. TABET-DERRAZ, Z. KEBBAB, C. MATHIEU, B. KHELIFA, R. DESFEUX, *Thin Solid Films* **2006**, *497*, 58-64.
[44] R. R. AHIRE, B. R. SANKAPAL, C. D. LOKHANDE, *Mater. Res. Bull.* **2001**, *36*, 199-210.
[45] R. S. MANE, B. R. SANKAPAL, C. D. LOKHANDE, *Thin Solid Films* **2000**, *359*, 136-140.
[46] N. P. JU XU, XUEYAN WU, DANIELA IACOPINO, AIDAN J. QUINN, GARETH REDMOND, THOMAS BEIN, MICHAEL A. MORRIS AND JUSTIN D. HOLMES, *Small* **2006**, *in publication*.
[47] O. C. MONTEIRO, T. TRINDADE, J. H. PARK, O. B. P., *Chem. Vapor Depos.* **2000**, *6*, 230.
[48] Y. PENG, D. H. QIN, R. J. ZHOU, H. L. LI, *Mater. Sci. Eng. B-Solid State Mater. Adv. Technol.* 2000, 77, 246-249.

Single crystal nanowire arrays synthesis

Ju Xu, Nikolay Petkov, Daniela Iacopino[2], Aidan Quinn[2], Gareth Redmond[2],Thomas Bein[3], Michael A. Morris and Justin D. Holmes*

Oriented Growth of Single Crystalline Bi_2S_3 Nanowire Arrays

Oriented Single crystal nanowire arrays: Highly oriented single crystal Bi_2S_3 nanowire arrays were formed inside AAM templates using a new simple solventless approach. A high yield of pore filling of Bi_2S_3 nanowires inside the channels of the templates can be achieved by injection the melted single source precursor liquid into the channels followed by thermolysis. Using AAMs with different pore size, the diameters of nanowires can be easily controlled. The absorption profile (band-gap) of these nanowires was found to shift obviously to higher energies as the mean diameter of the nanowires decreased.

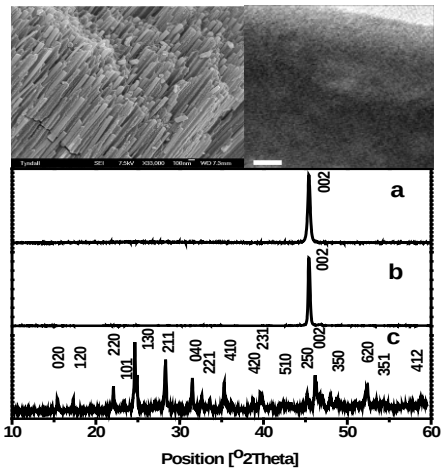

Supporting Information

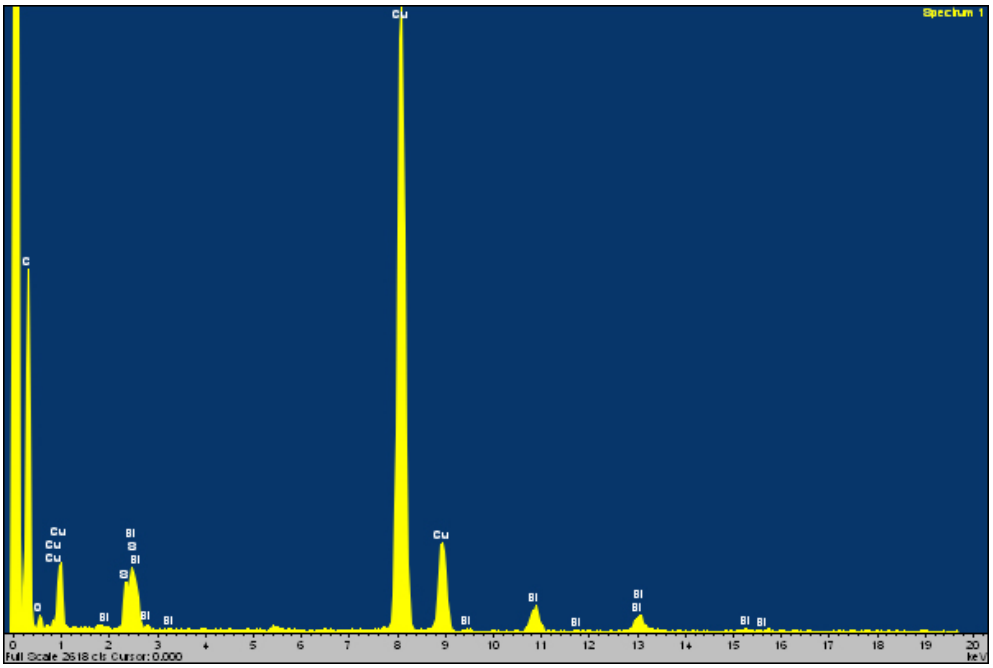

Figure S1 EDX analysis of Bi_2S_3 nanowires librated from AAM template,

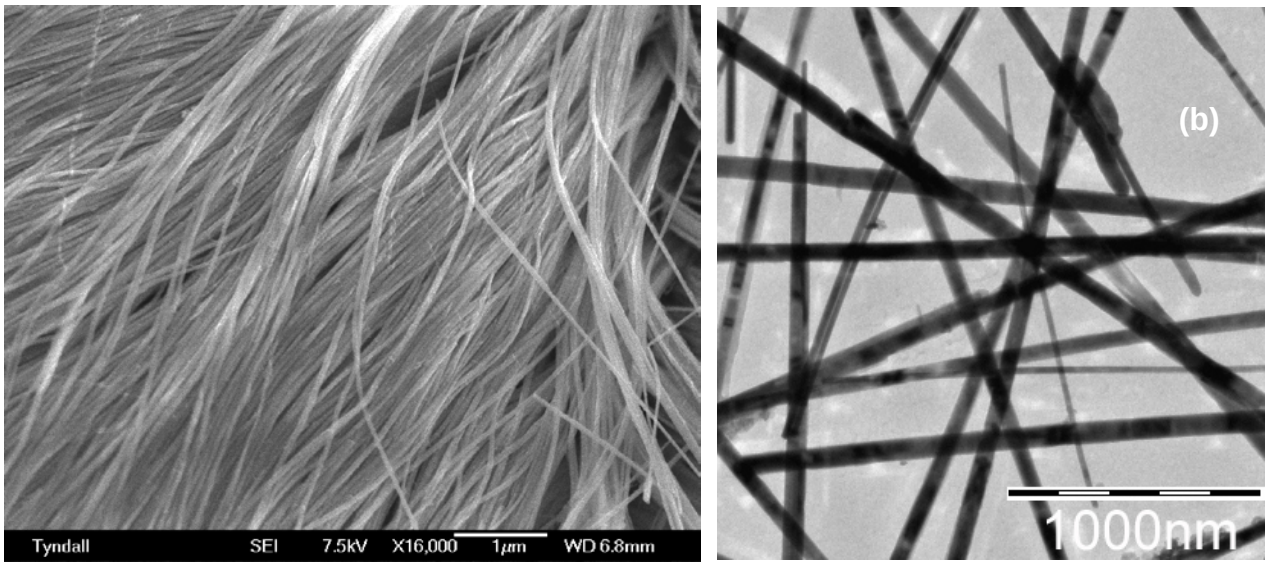

Figure S2 A large scale of Bi_2S_3 nanowires librated from 80nm AAM template a) SEM picture b) TEM picture

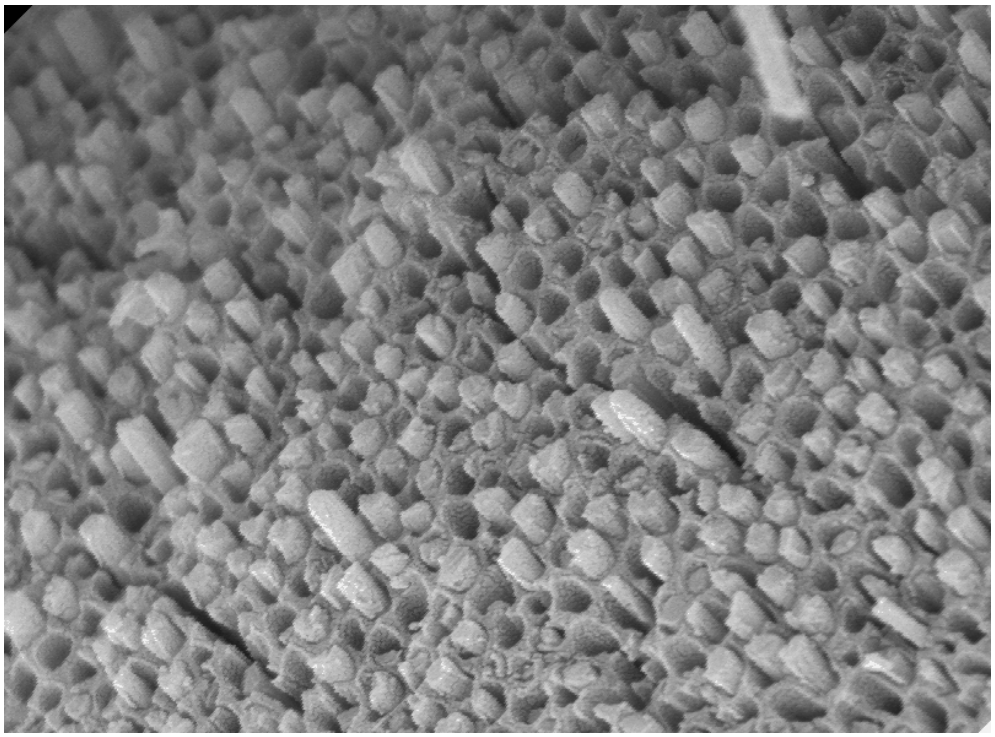

Figure S3 Plane-view SEM images of the Bi_2S_3 nanowire arrays within AAMs with mean pore diameters of 80 nm